# Simulations of Ti-Y-O Nanoclusters in Ferritic Alloys

A Thesis Presented for the

Master of Science

Degree

The University of Tennessee, Knoxville

Natalie Browning Camilli

May 2013

# DEDICATION

This thesis is dedicated first to God, who has saved me by His grace and not by my own works. Regardless of my accomplishments in this life, I have eternal hope in my faith and relationship with my Lord and Savior, Jesus Christ, as an excerpt from the book of Romans explains: "since we have been justified by faith, we have peace with God through our Lord Jesus Christ. Through him we have also obtained access by faith into this grace in which we stand, and we rejoice in hope of the glory of God." I would also like to dedicate this work to my husband, family, and friends for their unfailing love and support throughout my life and academic endeavors. Their encouraging words and unwavering belief in me were critical to my success.

# ACKNOWLEDGEMENTS

I would like to express my sincere gratitude to Drs. Brian Wirth and Karl Hammond for their guidance and support during my graduate research at the University of Tennessee. I would especially like to thank Karl Hammond for his guidance and help in each step of my journey toward completion of the research included in this thesis. It is through his help that I have learned the necessary information and computational techniques required for the research contained in this thesis. I would also like to thank Dr. Lawrence Heilbronn and Dr. G. Ivan Maldonado for serving on my graduate committee and for the wealth of knowledge I have gained from them throughout my undergraduate and graduate careers at the University of Tennessee.

# ABSTRACT

Nanostructured ferritic alloys possess high strength and resistance to radiation effects due to the presence of nanoprecipitates. Though nanostructured ferritic alloys have desirable mechanical properties, the exact composition and structure of the nanoprecipitates is unknown; thus, atomistic simulations involving the formation of nanoclusters give insight as to their structure. This thesis focuses on the structure, formation and radiation stability of Ti-Y-O [titanium-yttrium-oxygen] nanoclusters in iron. The activation energies for diffusion and the diffusion coefficients of oxygen interstitial atoms in iron are determined. The binding energies of various combinations of oxygen interstitial atoms and iron vacancies are also tabulated. Thermodynamic formation energies of Y-O and Ti-O nanoclusters are calculated. Also, the effects of radiation on Ti-Y-O clusters are studied using defect cascade simulations. Yttrium and titanium are found to provide stability in small oxygen clusters. Ti-Y-O clusters are found to exhibit resistance to radiation damage. Radiation effects are found to be minimal in instances in which the primary knock-on atom is a yttrium atom near the center or on the periphery of the Ti-Y-O precipitate cluster.

# TABLE OF CONTENTS

# List of Figures

# INTRODUCTION

Many new reactor designs such as the molten salt reactor, gas cooled fast reactor, and fusion reactor concepts implement higher temperatures than did previous designs. Also, higher radiation damage levels occur in new reactor concepts. Structural materials to be used in these new reactor designs must be able to withstand such harsh conditions. Therefore, advanced materials must be employed to ensure proper operation and reliability with increased temperature and radiation levels. Nanostructured ferritic alloys possess the mechanical properties necessary to survive in the type of environment proposed by Generation IV nuclear reactor designs [1].

Nanostructured ferritic alloys are iron alloys containing small solute clusters. These small clusters are one to three nanometers in size and improve the mechanical properties of iron in high-temperature and highly-irradiated environments. Some desirable features of these alloys are their ductility and corrosion resistance. Nanostructured ferritic alloys containing Ti-Y-O nanoclusters also exhibit strength in high-temperature environments due to their high concentration of titanium, yttrium, and oxygen precipitates. These alloys are also characterized by very fine grains and a high density of dislocations [2]. In addition to their strength at high temperatures, nanostructured ferritic alloys are resistant to long-term radiation damage due to a high density of microstructural sinks which inhibit defect accumulation [2].

An understanding of the structure and early stages of growth of Ti-Y-O nanoclusters in ferritic alloys is necessary for further modeling and research related to nanostructured ferritic alloys containing Ti, Y, and O. The detailed character of the nanoclusters and the events leading to their formation as well as their stability under long-term irradiation are not well understood [3]. Previous experimental work has been conducted concerning the formation of Ti-Y-O clusters in ferritic alloys, including small angle neutron scattering (SANS) and transmission electron microscopy (TEM) [3]. A previous study [3] has shown that titanium and yttrium are required for the formation of nanoclusters at high temperatures. Atom probe tomography (APT) studies have shown that Ti-Y-O clusters have high Ti to Y ratios up to 3:1 or more and that the number of Ti plus Y atoms is typically greater than the number of oxygen atoms present in the clusters [4]. A study by Alinger and colleagues experimentally determined the sequence of events leading to the formation of nanoclusters in iron, concluding that yttria is dissolved in metallic powders during mechanical alloying and that yttrium, oxygen, and titanium precipitate during hot consolidation [4]. However, this study did not allude to the exact structure and composition of the clusters. An experimental study [5] using APT showed that nanoclusters are very tolerant to neutron irradiation, stating that no significant changes in size or number density of the clusters were observed when exposed to neutron irradiation of 3 dpa.

The previous studies mentioned here were performed using experimental techniques. These studies were successful in documenting some details of the formation of precipitate clusters, such as the mechanisms by which they form under mechanical alloying and their general behavior under irradiative environments. Though previous work has

gained significant ground in the study of nanostructured ferritic alloys, there is no comprehensive understanding of the structure and composition of Ti-Y-O clusters. This work will serve to lay the groundwork for a more extensive understanding of the formation of small precipitate cluster of Ti, Y, and O in iron. The work included in this thesis also examines on a microscopic level the effects of radiation on Ti-Y-O clusters in iron. The use of molecular dynamics simulations allows a study of the formation of clusters and their characteristics and structure on a microscopic level.

It is desired to understand and document the binding energies of iron vacancies and oxygen interstitials, since O-vacancy binding could play an important role in stabilizing clusters [2]. It is also advantageous to study the diffusivities of oxygen interstitial atoms in iron; the ability of the oxygen atoms to diffuse through the iron lattice influences the growth of the cluster. Furthermore, studies of the early stages of formation of nanoclusters are beneficial in that they give insight as to their composition and structure. It is also useful to study how incident radiation affects Ti-Y-O nanoclusters in iron.

This work investigates mechanical properties of nanostructured ferritic alloys. The research in this work sheds light on the structure and formation of Ti-Y-O clusters in iron. The work presented in this thesis examines the diffusivities of oxygen interstitial atoms in body-centered cubic iron and the activation energy for oxygen diffusion in iron. This research also studies the binding energies of oxygen atoms and iron vacancies based on the chosen energy model [6]. The thermodynamic formation energies of Ti-O and Y-O clusters are also studied and documented. Small clusters of titanium, yttrium, and oxygen are studied to determine the threshold temperatures at which they are no longer bound. Also

in this work, Ti-Y-O nanoclusters are subjected to incident radiation in order to study the behavior of the NFA under irradiative environments. An overview of the molecular dynamics simulations used in the work presented in this thesis follows.

# CHAPTER 1:
# COMPUTATIONAL METHOD

## 1.1 MOLECULAR DYNAMICS (MD) SIMULATIONS

Molecular dynamics (MD) simulations are an efficient tool in studying the formation of Ti-Y-O nanoclusters in iron. These simulations run much more quickly than first principles based electron structure calculations such as density functional theory (DFT) and, therefore, are less costly due to the required computing time. MD simulations also provide a more intimate view of the formation of clusters than do experimental studies. While TEM studies are limited to 5-nm precipitate clusters, MD allows for the study of smaller, 1-3 nm clusters. In addition, MD simulations can efficiently model systems containing only a few atoms as well as systems with a large number of atoms. In order to aid in the discussion of MD simulations, Figure 1 contains a flow chart explaining the steps involved in a molecular dynamics simulation.

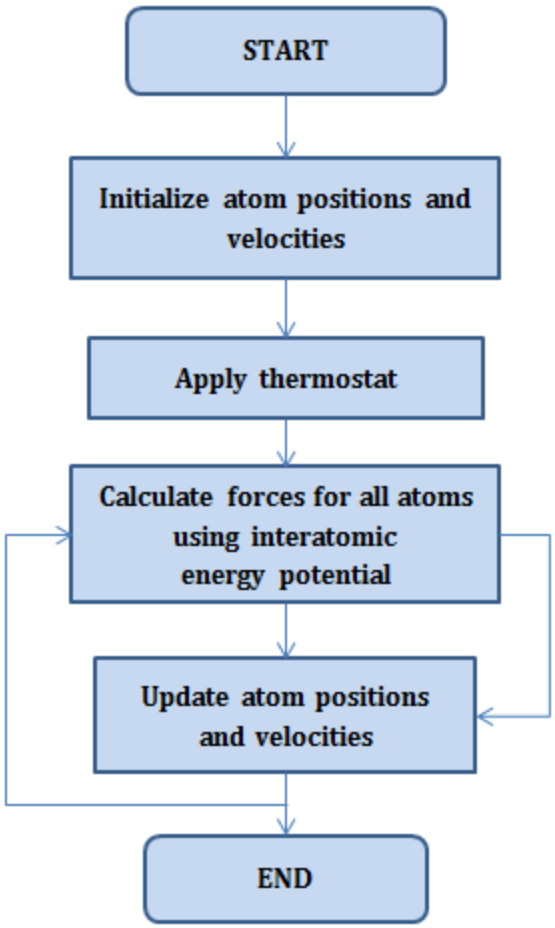


Figure 1. Flow chart explaining steps used in molecular dynamics simulations

As shown in Figure 1, a molecular dynamics simulation is set up by first initializing the positions and velocities of the atoms. A simulation box is created with a certain height, width, and depth. Atoms are placed within the simulation box, and their atomic weights and initial velocities are assigned. A requested temperature is entered, and an ensemble of velocities is generated and scaled to produce this temperature. A thermostat may be applied in order to maintain or establish an acceptable temperature prior to running the simulation. The thermostat controls the temperature of the simulation by comparing the

temperature from the previous time step and adjusting the velocities accordingly. The force is calculated for each atom in the simulation based on the interatomic energy potential. Minimizations are then performed, and the positions and velocities of the atoms in the simulation are updated. The forces are then calculated once again, and the cycle continues until an acceptance criterion has been met based on the energy of the system.

## 1.2 LARGE-SCALE ATOMIC/MOLECULAR MASSIVELY PARALLEL SIMULATOR (LAMMPS)

LAMMPS (Large-scale Atomic/Molecular Massively Parallel Simulator) is a classical molecular dynamics simulation code, developed by Sandia National Laboratories [7]. LAMMPS integrates Newton's equations of motion for a collection of atoms. This code is able to model an ensemble of particles with a variety of force fields and boundary conditions, including both two- and three-dimensional systems. The use of periodic boundary conditions in LAMMPS allows for the number of atoms in a simulation to be conserved; no atoms are lost through the boundaries in a simulation using periodic boundary conditions. LAMMPS uses neighbor lists to track nearby atoms; these lists are optimized for systems with particles which are repulsive at short distances in order to assure that the local density of particles does not become too large [7].

The LAMMPS code has the ability to run on parallel computers; the use of multiple processes allows LAMMPS to efficiently models systems with a large number of particles. LAMMPS uses spatial-decomposition techniques to partition the simulation domain into smaller three-dimensional sub-domains which are assigned to individual processors [7].

LAMMPS uses interatomic pair potentials, which describe how atoms in the simulation interact with one other on a pair-wise basis.

## 1.3 Interatomic Energy Potentials

Previous atomistic simulations of Ti-Y-O nanoclusters have been performed using density functional theory, or DFT. Simulations using DFT are very time-consuming. However, the same type of calculation can be performed using molecular dynamics simulations which implement interatomic energy potentials. For example, a simulation using energy potentials could take a few minutes, while the same type of simulation using DFT could take months to complete. In a previous study [2], the thermodynamic formation energies of small oxide clusters in iron were calculated using DFT. It is useful to calculate the formation energies of nanoclusters using interatomic energy potentials since these types of simulations are less costly due to computer time and in order to validate the interatomic potentials [6] used in the studies in this thesis.

The interaction between any pair of atoms is defined by interatomic energy potentials which are interpolated from a table of energy potentials based on the distance between atoms. For the research conducted for this thesis, the interatomic energy potentials used were those created by Karl D. Hammond of the Wirth Research Group [6]. These interatomic potentials are pairwise potentials for a system containing iron, yttrium, titanium, and oxygen. The interatomic potentials were developed using the Born-Mayer

potential to represent Pauli repulsion of electron clouds for small distances and coupled with an attractive term accounting for van der Waals attractions at long ranges [6]. The mathematical representation of the interatomic potentials is as follows:

$$V(r) = \begin{cases} V_{ZBL}(r) + dE & r \leq r_1 \\ \sum_{n=0}^{5} s_n r^n & r \in (r_1, r_2) \\ V_{Buckingham}(r) f_{cut}(r) & r \geq r_2 \end{cases} \quad (1a)$$

$$V_{ZBL}(r) = \frac{K_C Z_1 Z_2 q_e^2}{r} \phi(r/a_u) \quad (1b)$$

$$\phi(x) = 0.1818e^{-3.2x} + 0.5099e^{-0.9423x} + 0.2802e^{-0.4029x} + 0.02817e^{-0.2016x} \quad (1c)$$

$$a_u = \frac{0.8854 a_0}{Z_1^{0.23} + Z_2^{0.23}} \quad (1d)$$

$$V_{Buckingham}(r) = Ae^{-r/\rho} - Cr^{-6} \quad (1e)$$

$$f_{cut}(r) = \begin{cases} 1 & r \leq R - D \\ \frac{1}{2} - \frac{1}{2}\sin\left(\frac{\pi}{2}\frac{r-R}{D}\right) & |r - R| < D \\ 0 & r \geq R + D \end{cases} \quad (1f)$$

where $r$ is the distance in angstroms between two atoms, $a_0$ is the Bohr radius, $K_C$ is Coulomb's constant, $q_e$ is the electron charge, and $Z_i$ is the atomic number of species $i$. $V_{ZBL}$ refers to the universal repulsive potential of Ziegler, Biersack, and Littmark, and $V_{Buckingham}$ to the pairwise interaction form suggested by Buckingham. [6]

The joined Buckingham-ZBL potentials are a useful model of energy potentials for systems of iron, titanium, yttrium, and oxygen [6]. These interatomic potentials were used in simulations for the purposes of this thesis. When used in Ti-Y-O cluster simulations, the

interatomic potential at a given energy was interpolated from the table of potentials based on the distance between two atoms.

# CHAPTER 2:
# INVESTIGATION OF THE KINETICS GOVERNING THE FORMATION OF TI-Y-O CLUSTERS

## 2.1 OXYGEN INTERSTITIAL DIFFUSIVITY IN IRON

In order to gain a more complete understanding of the mechanisms by which Ti-Y-O clusters form in an iron matrix, it was desired to study and document the diffusivity of oxygen atoms in body-centered cubic iron. The mobility of oxygen atoms in iron is an important factor in the formation and growth of small precipitate clusters in iron. The ability of oxygen to diffuse in the iron lattice is a key component in cluster formation.

To calculate the diffusivity of oxygen interstitial atoms within body-centered cubic iron, simulations were performed in which interstitial oxygen atoms were allowed to diffuse in an iron lattice. The simulation box was created as a 20 x 20 x 20 box, which means the simulation box was 20 times the lattice parameter of body-centered cubic iron, or 20 x 2.8665 Å in the x, y, and z-directions. This simulation box was filled with on-lattice iron atoms. The oxygen atoms were then placed at interstitial sites within the simulation box. The simulations contained 16,000 iron atoms and 1 or 2 oxygen atoms for single or di-oxygen interstitial diffusion, respectively.

The velocities of the atoms in the simulation were created using a temperature seed and random number seed. The atoms were then assigned velocities using a Gaussian distribution with a mean of 0.0 and the appropriate sigma required to produce the temperature requested in the input. Two simulations were performed: one involved a

single interstitial oxygen atom diffusing in iron and the other a di-oxygen interstitial diffusing in iron. For each simulation, five versions were run, each with a different random number seed. Each simulation was run for a time of 5 ns, and the coordinates of the oxygen atoms were saved at 0.5-picosecond intervals. The mean-square displacement was then calculated from this data. The averaged mean-square displacement data over five simulations for single oxygen and a di-oxygen interstitial are plotted against the simulation time in Figure 2 and Figure 3.

To calculate the mean-square displacement, the following equation was used:

$$MSD = \langle |r(t) - r(0)|^2 \rangle \tag{2.1a}$$

The mean square displacement is calculated as the displacement averaged over all atoms and time. To calculate the mean-square displacement according to Equation 2.1a, the following procedure was followed:

$$dx_i^2 = \frac{2}{n}\big(x(j+i) - x(j)\big)^2 + dx_i^2 \tag{2.1b}$$

$$dy_i^2 = \frac{2}{n}\big(y(j+i) - y(j)\big)^2 + dy_i^2 \tag{2.1c}$$

$$dz_i^2 = \frac{2}{n}\big(z(j+i) - z(j)\big)^2 + dz_i^2 \tag{2.1d}$$

$$dr^2 = |r(t) - r(0)|^2 = dx^2 + dy^2 + dz^2 \tag{2.1e}$$

In Equation 2.1, *n* refers to the number of time steps in the simulation. The quantities $dx^2$, $dy^2$, and $dz^2$ are the x, y, and z components of the mean-square displacement. The distances between the x, y, and z-coordinates of an atom's location at time step *t+1* and

time step *t* are calculated in Equations 2.1b-d. Time *t* is represented by the letter *j*, and time step *t+1* is represented by *j+i*. The value of the sum of the previous iterations is added to the value of the present iteration for each calculation of $dx_i^2$, $dy_i^2$, and $dz_i^2$. The mean-square displacement is then calculated as the sum of the squares of the x, y, and z components.

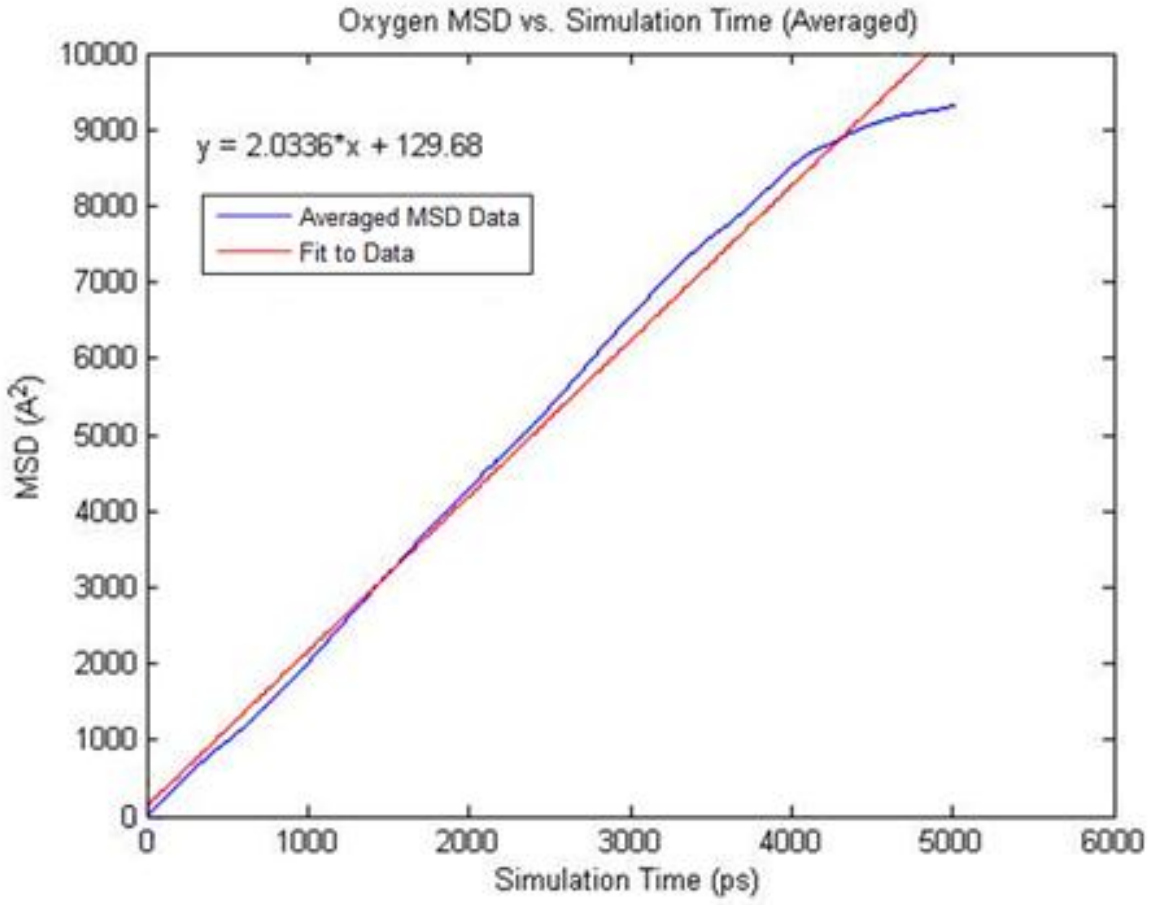


Figure 2. Mean-square displacement vs. simulation time for single oxygen interstitial diffusion in BCC iron

In Figure 2, the blue line corresponds to the mean square displacement data averaged across five simulations, and the red line depicts the linear fit to the data. The equation of the linear fit is shown in the figure. The diffusion coefficient was determined from this linear fit to the mean-square displacement vs. simulation time data.

The linear fit to the data in Figure 2 estimates the slope of the fit to the averaged mean square displacement vs. simulation time data to be 2.03 $A^2$/ps. According to the Einstein Equation [8], the following relationship is valid:

$$\langle x^2 \rangle = q_i D t \tag{2.2}$$

Where:

$\langle x^2 \rangle$ = mean-square displacement

$q_i$ = dimensionality constant = 2 if 1-dimensional diffusion
4 if 2-dimensional diffusion
6 if 3-dimensional diffusion

$D$ = diffusion coefficient

$t$ = time

Applying Equation 2.2 to the slope of the linear fit shown in Figure 2, the resulting value of the diffusion coefficient is $3.4 \times 10^{-5}$ $cm^2 s^{-1}$. Thus, this is the value of the diffusion coefficient of a single interstitial oxygen atom in body-centered cubic iron at 2500 K.

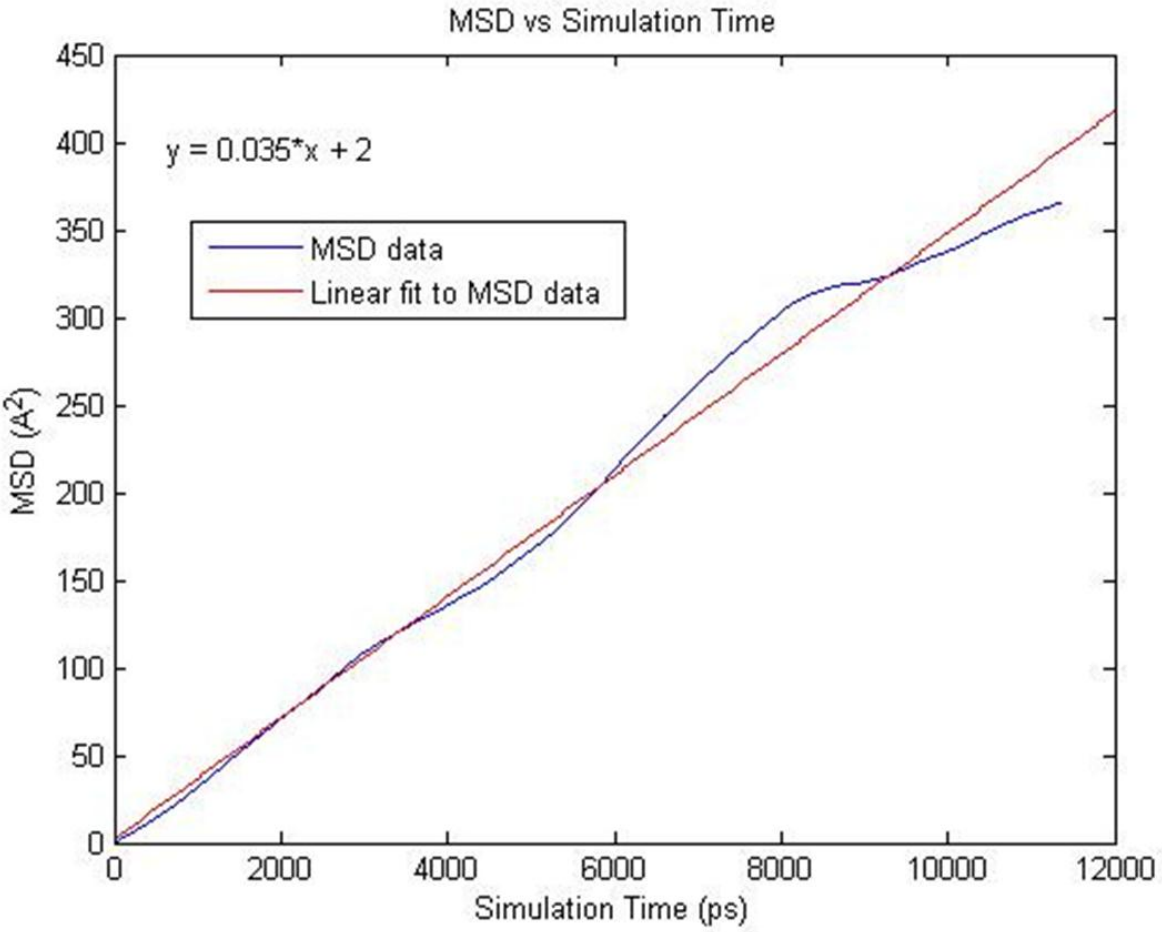


Figure 3. Mean-square displacement vs. simulation time for di-oxygen interstitial diffusion in BCC iron

In Figure 3, the blue line shows the averaged mean-square displacement data for a di-oxygen interstitial atom diffusing in BCC iron. The red line shows a linear fit to the data. The slope of the linear fit to the data is 0.035; applying Equation 2.2, the diffusion coefficient is then found to be $5.80 \times 10^{-7}$ $cm^2s^{-1}$ at 1000 K.

Comparing the diffusion coefficients of the single and di-oxygen interstitial atoms in iron, the single interstitial oxygen atom diffusion coefficient is about 60 times that of the di-oxygen diffusion coefficient. Single interstitial oxygen atoms are much more mobile in an iron matrix than are di-oxygen interstitial pairs. These data can be compared to documented values for the diffusivity of oxygen in iron using the Landolt-Börnstein database reference 69B [9]. According to the database, the diffusion coefficient of oxygen in iron can be calculated over the entire alpha-range using the following equation:

$$\log D\ [m^2 s^{-1}] = -5.948 - 0.4334X + 6.08 \times 10^{-4} X^2, \quad where\ X = \frac{10^4}{T} \qquad (2.3)$$

Substituting the temperatures used in the single and di-oxygen interstitial diffusivity calculations into Equation 2.3, the values of the diffusivity are calculated as 2.12 x $10^{-4}$ $cm^2 s^{-1}$ at 2500 K and 6.01 x $10^{-7}$ $cm^2 s^{-1}$ at 1000 K. These values align well with the values calculated using the simple pairwise energy potentials described in Chapter 1.3. The diffusion coefficient values agree more for the 1000K calculation that for the 2300 K calculation. Table 1 shows the comparisons of the values as calculated using the pairwise potentials and the Landolt-Börnstein database.

Table 1. Comparison of diffusion coefficients of oxygen in iron calculated using pairwise interatomic energy potentials and those calculated using Landolt-Börnstein data

| Temperature | *D* [pairwise potentials] | *D* [Landolt-Börnstein data] |
|---|---|---|
| 1000 K | $5.80 \times 10^{-7}$ $cm^2s^{-1}$ | $6.01 \times 10^{-7}$ $cm^2s^{-1}$ |
| 2500 K | $3.4 \times 10^{-5}$ $cm^2s^{-1}$ | $2.12 \times 10^{-4}$ $cm^2s^{-1}$ |

## 2.2 Arrhenius Plots: Oxygen Diffusivity in Iron

Using the same procedure outlined in the previous section, multiple simulations were run in LAMMPS in which a single or di-oxygen interstitial atom diffused in an iron lattice. The simulations were run at varying temperatures, ranging from 800 K to 2500 K. The maximum temperature of the di-oxygen study was lower than that for the single oxygen study because the di-oxygen pair dissociates at higher temperatures. The diffusion coefficient was determined for each of the temperatures using Equation 2.2. The logarithm of the diffusion coefficient was then plotted against the inverse of the temperature. The resulting plot is shown in Figure 4.

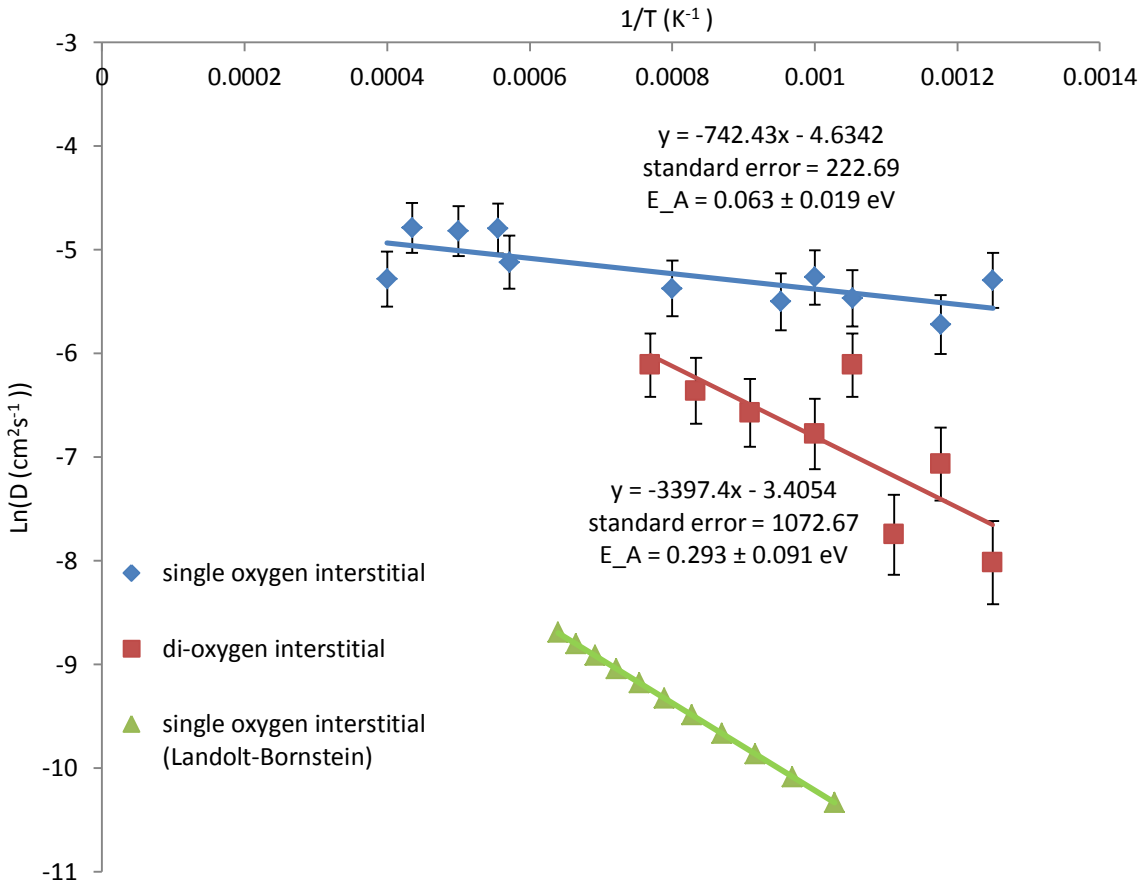


Figure 4. Arrhenius plot of single and di-oxygen interstitial diffusivities in BCC iron

The slope of the logarithm of the diffusion coefficient versus the inverse of temperature for a single interstitial oxygen atom is -742 with a standard error of 222.69. This slope is proportional to the activation energy for diffusion by Boltzmann's constant. This relationship is shown in Equation 2.4.

$$E_A = m * k \tag{2.4}$$

Where:

$E_A$ = Activation energy for diffusion

$m$ = slope of the fit to logarithm of diffusion coefficient vs. inverse temperature data

$k$ = Boltzmann constant = 8.6173324 x $10^{-5}$ $eVK^{-1}$.

Substituting the slope of the linear fit to the data into Equation 2.4, the activation energy for diffusion of a single oxygen interstitial atom in iron was found to be 0.063 ± 0.019 eV. This value differs significantly from the Landolt-Börnstein data [9]; the MD simulation predicts an activation energy of 0.06 eV, whereas the experimental value for the activation energy is approximately 0.8 eV.

The slope of the fit to the di-oxygen interstitial data is -3397 with a standard error of 1073. Applying Equation 2.3 to the slope of the fit, the activation energy is found to be 0.293 ± 0.091 eV. Thus, the activation energy for diffusion for a di-oxygen interstitial in iron is larger than for a single interstitial oxygen atom in iron. The activation energy is related to the diffusion coefficient by the following equation:

$$D = D_0 e^{-\frac{E_A}{kT}} \tag{2.5}$$

In Equation 2.5, $D$ is the diffusion coefficient, $D_0$ is a pre-exponential representing the maximum theoretical diffusion coefficient at an infinite temperature, $E_A$ is the activation energy for diffusion, $T$ is the temperature, and $k$ is Boltzmann's constant. The probability of thermal fluctuations overcoming the energy barrier for diffusion is shown by Equation 2.6.

$$R_j = R_0 e^{-\frac{E_A}{kT}} \tag{2.6}$$

In Equation 2.5, the probability of thermal vibrations causing enough energy to overcome the barrier to diffusion is represented as $R_j$. $R_0$ represents the attempt frequency which is related to the frequency of atomic vibrations. The atomic vibrations or thermal energy of atoms are typically much smaller than the activation energy required to break the bonds with neighboring atoms and migrate to adjacent sites. Thus, the energy of atoms within a small volume must be pooled together in order to overcome the activation barrier. This is why diffusion is represented as a probability of overcoming this barrier. In examining Equations 2.5 and 2.6, it is obvious that the higher the activation energy, the smaller the diffusivity and the lower the probability of atomic diffusion. Therefore, there is a higher probability of atomic diffusion for a single interstitial oxygen atom than for a di-oxygen interstitial pair in body-centered cubic iron.

## 2.3 Oxygen-Iron Vacancy Binding Energy

Simulations used in oxygen-iron vacancy binding energy calculations were set up by first creating a 20 x 20 x 20 simulation box and filling it with BCC iron (lattice parameter = 2.8665 Å). An iron vacancy was either created by deleting an on-lattice iron atom or by creating a substitutional oxygen atom on a lattice site and deleting the overlapping iron atom. Oxygen atoms were either created at interstitial sites or as substitutional atoms. Two or more oxygen atoms and/or vacancies were placed within an iron lattice far enough apart to be considered infinitely far apart. This means that when the entities were moved further apart, there was no significant change in energy. The total potential energy of the system

with the atoms and/or vacancies far enough apart to prevent interaction was recorded. Then, the same simulation was run with the two or more entities placed at neighboring sites, and the energy of the system was also recorded under this condition. The binding energy was then calculated as the difference in energies of the system with the entities considered infinitely far apart and that with the entities at neighboring sites. This calculation is shown in Equation 2.6.

$$BE = E_{inf} - E_{neighbor} \tag{2.6}$$

In Equation 2.6, $E_{inf}$ is the total potential energy of the system when the entities in question are separated enough to be considered infinitely far apart or prevent interaction. The term $E_{neighbor}$ refers to the total potential energy of the system with the entities of interest at neighboring sites within the simulation box. The binding energy is the difference between these two energies. For the purpose of this thesis, a positive binding energy corresponds to a bound system, and a negative binding energy to an unbound system. Using Equation 2.6, a table of binding energies was produced for many combinations of oxygen atoms and iron vacancies. The results of the calculations are shown in Table 2.

Table 2. Oxygen-iron vacancy binding energies (eV)

| | | # of Fe Vacancies | | | |
|---|---|---|---|---|---|
| # of O(i) atoms | # of O(s) atoms | 0 | 1 | 2 | 3 |
| 0 | 0 | | | 0.7 | 1.4 |
| 0 | 1 | | | 0.73 | 0.29 |
| 1 | 0 | | 0.41 | 1.14 | 0.29 |
| 1 | 1 | | 1.08 | 1.17 | 7.27 |
| 2 | 0 | 1.70 | 2.32 | 0.29 | 0.46 |
| 0 | 2 | | | 0.66 | 2.17 |
| 3 | 0 | 1.96 | 0.48 | 2.28 | 1.99 |
| 2 | 1 | | 0.21 | 0.03 | 1.3 |
| 1 | 2 | | | 0.94 | 1.37 |
| 0 | 3 | | | | 1.65 |

From Table 2, the binding energy of two iron vacancies is 0.7 eV, whereas the binding energy of three iron vacancies is 1.4 eV, or twice that of two vacancies. Also, the binding energy of two substitutional oxygen atoms and two iron vacancies is 0.66 eV, which more than triples when an additional iron vacancy is introduced. An increase in binding energies is noticed for most increases in the number of vacancies. The binding energy is

small for an interstitial oxygen atom and iron vacancy; thus, there is a high likelihood of dissociation of this pair. This binding energy increases when the vacancy is the result of introducing a substitutional oxygen atom. Atomistic simulations were performed involving some of the clusters shown in Table 2. The results of these simulations are shown in the following section.

## 2.4 Small Ti-Y-O Cluster Simulations

Simulations of various clusters were performed in LAMMPS in which the temperatures were raised to determine under what circumstances the clusters dissociated. The clusters were a di-oxygen pair with a nearby iron vacancy, two oxygen interstitials with a nearby titanium atom, and two oxygen interstitials with a nearby yttrium atom. These clusters were placed in an iron lattice and given a velocity based on the temperatures set for each simulation; the simulations were run for 5 nanoseconds. From the simulations, movies were made in which the atoms either stayed bound or dissociated. Snapshots of these movies are shown in Figure 5, Figure 6, and Figure 7.

(a) (b)

Figure 5. Di-oxygen interstitial pair with a nearby iron vacancy at 1000 K (a) and 1700 K (b)

Figure 5 shows two interstitial oxygen atoms and a nearby iron vacancy. The red atoms represent interstitial oxygen atoms. The green atoms represent off-lattice iron atoms, and the black spheres represent iron vacancies. Figure 5a shows the cluster at 1000 K. At 1000 K, the oxygen atoms are bound by the iron vacancy. In Figure 5b, the temperature is 1700 K. At this temperature, the oxygen atoms are no longer bound by the iron vacancy, and the oxygen atoms begin to dissociate. Therefore, the di-oxygen interstitial pair with a nearby iron vacancy is not bound at 1700 K on the 5-nanosecond time scale of this simulation.

(a) (b)

Figure 6. Two oxygen interstitial atoms with a nearby titanium atom at 1000 K (a) and 1700 K (b)

Figure 6 shows snapshots of the simulation of two interstitial oxygen atoms and a nearby titanium atom. The red atoms represent interstitial oxygen atoms, and the blue atoms represent titanium. In Figure 6a, the oxygen atoms are bound to the titanium atom at 1000 K. In Figure 6b, the temperature of the simulation is 1700 K and the oxygen atoms are no longer bound to the titanium atom and begin to dissociate. A di-oxygen interstitial pair with a nearby titanium atom is not bound at 1700 K on the 5-nanosecond time scale of this simulation.

(a) (b)

Figure 7. Two oxygen interstitial atoms with a nearby yttrium atom at 1000 K (a) and 1700 K (b)

Figure 7 shows two snapshots from the simulations of two interstitial oxygen atoms with a nearby yttrium atom. Figure 7a shows a snapshot of the simulation at 1000 K; here, the oxygen atoms are bound to the yttrium atom. This is consistent with the previous two simulations in that the oxygen is bound at 1000 K. In Figure 7b, the snapshot of the simulation shows the oxygen atoms are still bound to the yttrium atom at 1700 K. In the simulations of two interstitial oxygen atoms with a nearby iron vacancy or a nearby titanium atom, the oxygen dissociated at 1700 K. Thus, on a 5-nanosecond time scale, the oxygen is bound at 1700 K when an yttrium atom is present.

Simulations were also run in which three oxygen interstitial atoms were allowed to diffuse in an iron lattice at a temperature of 1200 K. The first simulation involved only the three oxygen interstitial atoms, where the other simulations involved oxygen interstitials as well as one, two, or three iron vacancies. Movies were produced from these simulations in order to determine whether the oxygen atoms remained bound or dissociated from one another throughout the simulations. The results of these simulations are shown in Figure 8, Figure 9, and Figure 10.

(a) (b) (c) (d)

Figure 8. Sequential snapshots of tri-oxygen interstitial simulation at 1200 K at 1, 2, 3, and 4 nanoseconds

Figure 8 shows a sequence of snapshots taken from the movie generated by the simulation of three interstitial oxygen atoms in iron. In part (a), the three oxygen atoms are beginning to dissociate; two oxygen interstitials are still bound, but one has separated from the cluster. In part (b), the dissociated oxygen interstitial atom has moved further from the other two atoms. As the movie progresses, part (c) shows the three interstitial oxygen atoms have completely dissociated from one another. In part (d), the three atoms move even further apart. The snapshots in Figure 8 show that, unlike a di-oxygen interstitial, the tri-oxygen interstitial cluster is not bound at 1200 K.

(a) (b) (c)

Figure 9. Sequential snapshots of tri-oxygen interstitial with iron vacancy at 1200 K at 2, 3, and 4 nanoseconds

Figure 9 shows a sequence of snapshots taken from the movie generated by the simulation of three interstitial oxygen atoms with a nearby iron vacancy. In part (a), two of the three oxygen atoms are bound to the iron vacancy, and the third oxygen atom is dissociated from the cluster. In part (b), the dissociated oxygen atom has moved further from the two oxygen atoms and iron vacancy. Part (c) shows the dissociated oxygen atom continuing to migrate from the two bound oxygen atoms and vacancy. From the snapshots in Figure 9, the presence of an iron vacancy does not cause the three oxygen interstitial atoms to be bound at 1200 K. However, with the presence of an iron vacancy, two of the three oxygen atoms remain bound at 1200 K as demonstrated in the simulations of a di-oxygen interstitial with a nearby iron vacancy at 1200 K.

(a) (b) (c) (d)

Figure 10. Sequential snapshots of tri-oxygen interstitial with two iron vacancies at 1200 K at 1, 2, 3, and 4 nanoseconds

Figure 10 shows snapshots of the simulation of a tri-oxygen interstitial cluster and two iron vacancies. Part (a) shows the three oxygen atoms and two iron vacancies in a cluster. As the simulation progresses, one oxygen atom dissociates from cluster, as shown in part (b). Part (c) then shows the three oxygen atoms have moved back toward one of the iron vacancies, but the other vacancy is not part of the cluster. As the simulation progresses, part (d) shows a cluster consisting of only two oxygen atoms and one iron vacancy, while the remaining oxygen atom and iron vacancy have dissociated from the other atoms. This simulation serves to further emphasize that two oxygen interstitial atoms are bound to an iron vacancy at 1200 K, but three oxygen atoms are not bound, even with the presence of an additional iron vacancy. It is important to note that the results of these simulations are based on simulations run for a finite time of 5 nanoseconds. These results offer a preliminary view of the types of temperatures for which the small oxygen clusters remain bound, but future work should be done to characterize the probability of dissociation at a particular temperature as a function of time.

# CHAPTER 3:
# STRUCTURE AND COMPOSITION OF TI-Y-O PRECIPITATE CLUSTERS

## 3.1 THERMODYNAMIC FORMATION ENERGIES OF Y-O AND TI-O CLUSTERS IN IRON

In order to evaluate the accuracy of the simple interatomic pair potentials described in the computational method section of this thesis, the formation energies of two structures were calculated and compared to a study performed by the University of Wisconsin [2]. The structures studied were "structure-matched" Y-O and Ti-O clusters based on the $Y_2O_3$ (yttria) and $TiO_2$ (titania) structures. The "structure-matching" method used in assembling Y-O and Ti-O clusters involved creating clusters which mimic yttrium and titanium oxides and embedding the structures in an iron matrix while creating as little distortion as possible to the oxide as well as to the surrounding iron matrix. Iron atoms which encroach upon the cluster were removed, resulting in strained clusters embedded in a strained iron matrix. In order to aid in the explanation of the "structure-matching" method used in assembling Y-O and Ti-O clusters, an illustration of the method is provided for an arbitrary metal oxide in Figure 11.

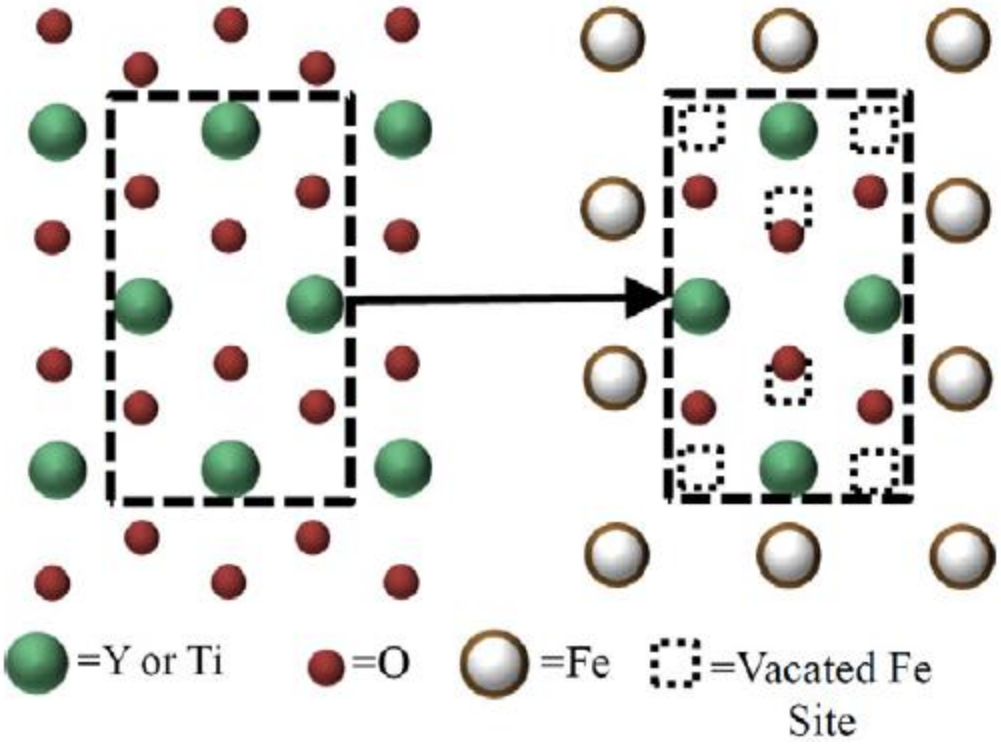


Figure 11. Arbitrary illustration of structure-matching method, figure from [2]

In creating a structure-matched Y-O cluster, the face centers of a two-by-two-by-two BCC iron supercell were replaced with yttrium, creating a yttrium octahedron. Iron atoms interior to this octahedron were then removed, and oxygen atoms were placed in appropriate positions with respect to the yttrium atoms so as to mimic the bixbyite yttria structure. In creating a "structure-matched" Ti-O cluster in iron, the [0 1 0] and [0 0 1] directions of the titania structure are oriented along the [1 1 0] and [0 0 1] directions of the iron crystal, respectively [2]. The four iron atoms at the corners of the rectangle described by this plane were replaced by titanium atoms, and two additional titanium atoms were placed at the edge centers at positions (0, 0, 0.5) and (1, 1, 0.5) in the BCC iron cell [2]. The

oxygen atoms were then introduced at appropriate positions with respect to the titanium atoms in order to mimic the rutile titania structure. The resulting "structure-matched" Y-O and T-O clusters are shown in Figure 12 and Figure 13.

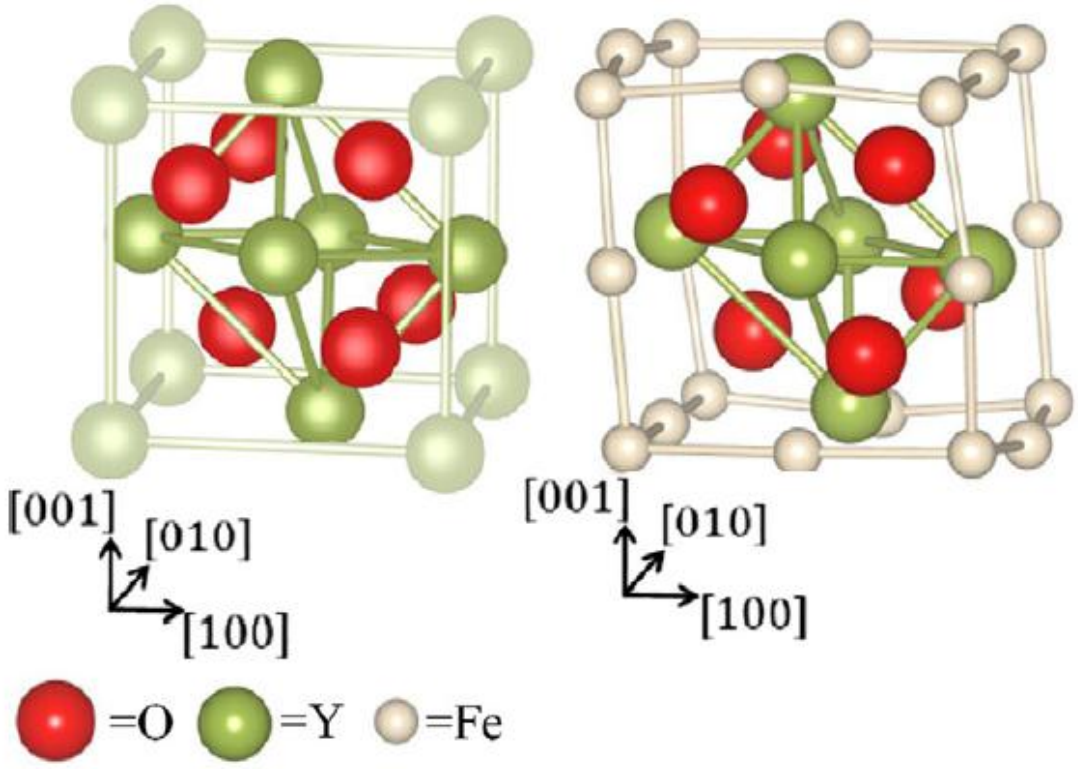


Figure 12. Structure-matched Y-O cluster (left) and Y-O cluster embedded in BCC iron (right), figure from [2]

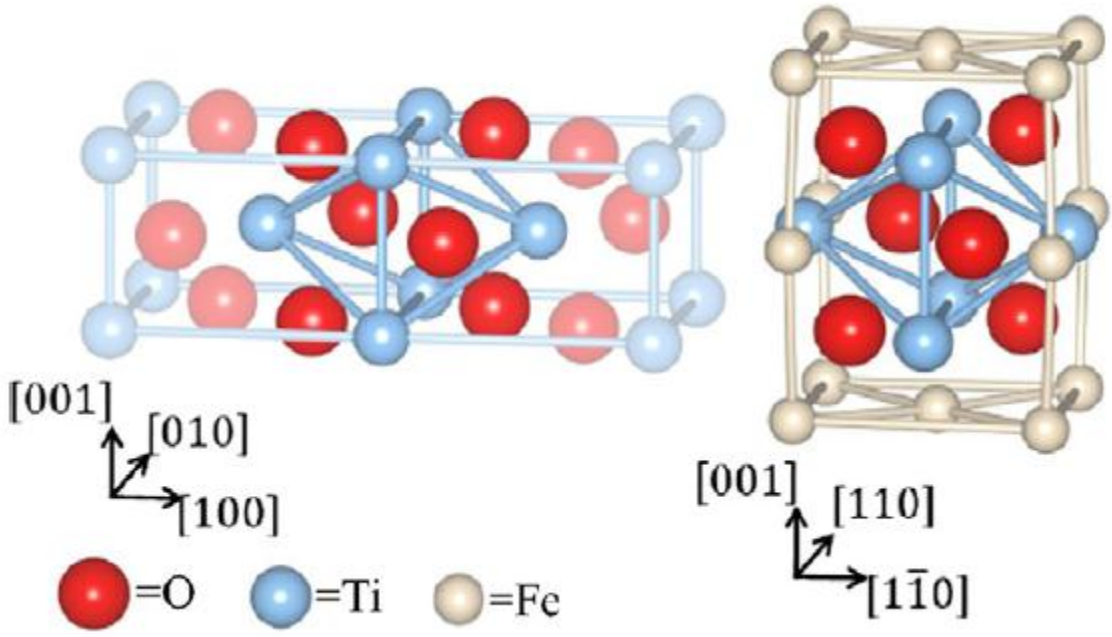


Figure 13. Structure-matched Ti-O cluster (left) and Ti-O cluster embedded in BCC iron (right), figure from [2]

To obtain the relaxed structures shown, the Y-O and Ti-O clusters were embedded in a 50 x 50 x 50 simulation box containing an iron matrix, and minimizations were performed to achieve full relaxation. The energy of the entire system with the Y-O or Ti-O cluster embedded in the iron matrix was recorded. Then, elemental Y, Ti, and O atoms were placed within the iron matrix to represent the dissolved state; care was taken in maintaining the same number of Fe, Ti, Y, and O atoms across simulations. The formation energy was then calculated as the difference in total potential energy between the clustered state and the dissolved sate, as shown in Equation 3.1. For the purposes of this thesis, positive formation energy corresponds to a bound system.

$$E_{formation} = E_{cluster} - E_{dissolved} \quad (3.1)$$

Multiple simulations were performed in calculating the formation energies of the previously described Y-O and Ti-O clusters in iron. Since oxygen diffuses many times faster in iron than do titanium and yttrium, for the time required for Ti or Y to form a cluster, equilibration with the local oxygen environment is nearly instantaneous [2]. As the cluster grows with each additional Y or Ti atom, oxygen is readily available to form a stable structure. For this reason, for a given number of yttrium or titanium atoms, the number of oxygen atoms in the cluster was varied. For each Y-O or Ti-O cluster, the formation energy was calculated using Equation 3.1. For comparison, the results of the study using DFT [2] are plotted along with the results of the simulations using the simple pairwise interatomic energy potentials in Figures 14 and 15.

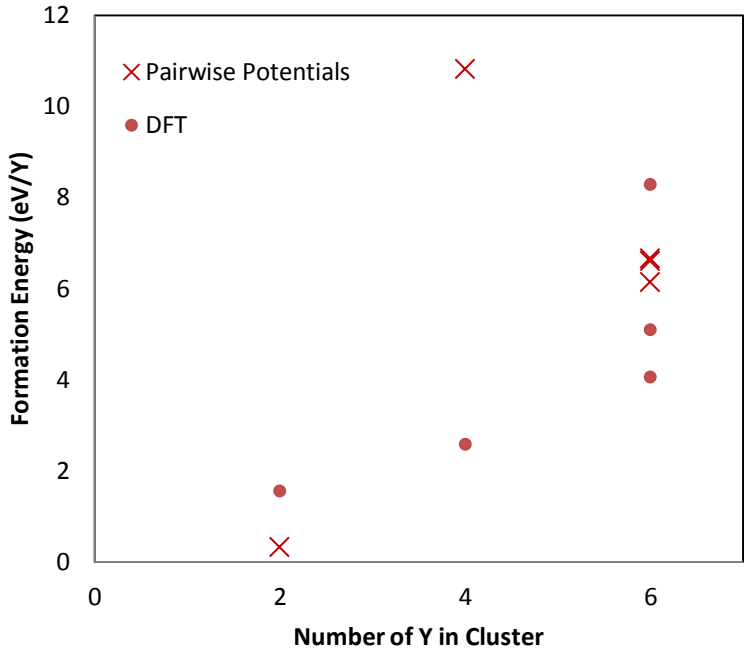


Figure 14. Formation energy as a function of the number of Y atoms in the cluster

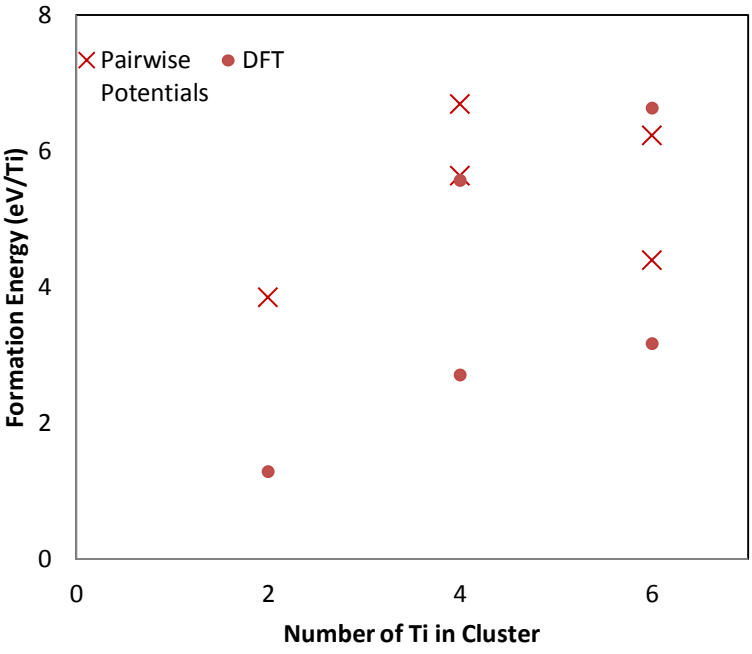


Figure 15. Formation energy as a function of the number of Ti atoms in the cluster

Figures 14 and 15 show that similar values of the cluster formation energies for various oxide clusters in iron were found using both density functional theory and the simple pairwise interatomic energy potentials described in the computational method section of this thesis. For the small Ti-O cluster containing two Ti atoms, the pairwise potentials appear to slightly overestimate the magnitude of the formation energy as compared to the DFT study. This is also true for the Ti-O cluster containing four Ti atoms and a varying number of oxygen atoms. The simple pairwise interatomic energy potentials seem to more closely reflect the formation energies as compared to DFT in the case of a Ti-O cluster containing six Ti atoms and a varied number of oxygen atoms. In the case of small Y-O clusters in iron, the formation energies calculated using pairwise energy potentials compare closely with those found using DFT except in the case of a Y-O cluster containing four Y atoms in which the pairwise potentials result in a much more negative formation energy.

In some cases, the structures used in the study using DFT [2] were not found to be the most stable configurations using the simple pairwise interatomic energy potentials. When the structures were minimized in LAMMPS, some structures changed significantly to reflect the most stable configuration with the lowest energy. For example, the Ti-O cluster containing two titanium atoms and three oxygen atoms is shown in Figure 16.

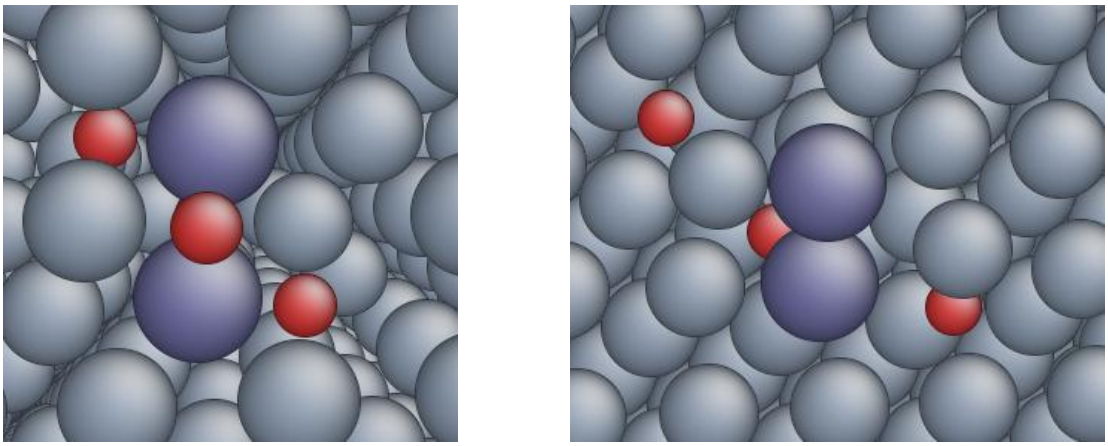

Figure 16. Ti-O cluster containing 2 Ti and 3 O atoms (left) and after relaxation (right)

In Figure 16, the red atoms represent oxygen while blue and grey atoms represent titanium and iron, respectively. The image on the left depicts the 3-O, 2-Ti cluster in iron as assembled using the "structure-matching" method. The image on the right shows the same structure after full relaxation using the pairwise energy potentials. As shown in the figure, the simple pairwise interatomic energy potentials predict a different configuration for the most stable 3-O, 2-Ti cluster in iron. Some of the variation in calculated formation energies is likely attributed to the differences in the minimal energy structures predicted by the

different potential models. In general, the simple pairwise interatomic energy potentials predict the most stable configurations for small Ti-O and Y-O clusters to be less compact than those assembled using the structure matching method previously described. Considering the differences in predicted lowest-energy structures, the formation energies of small titanium and yttrium oxide clusters embedded in iron are fairly consistent with the values documented in the Barnard study [2].

## 3.2 Lattice Monte Carlo: Off-lattice Relaxation of Ti-Y-O Clusters in Iron

An existing on-lattice simulation of a Ti-Y-O nanocluster in iron was used as a starting configuration for an off-lattice relaxation. In the on-lattice model, each atom is swapped with a nearest neighbor every time it is called upon. There is no concept of a rejected move using this algorithm. An example of the steps involved in an on-lattice simulation of a Ti-Y-O cluster in iron is shown in Figure 17.

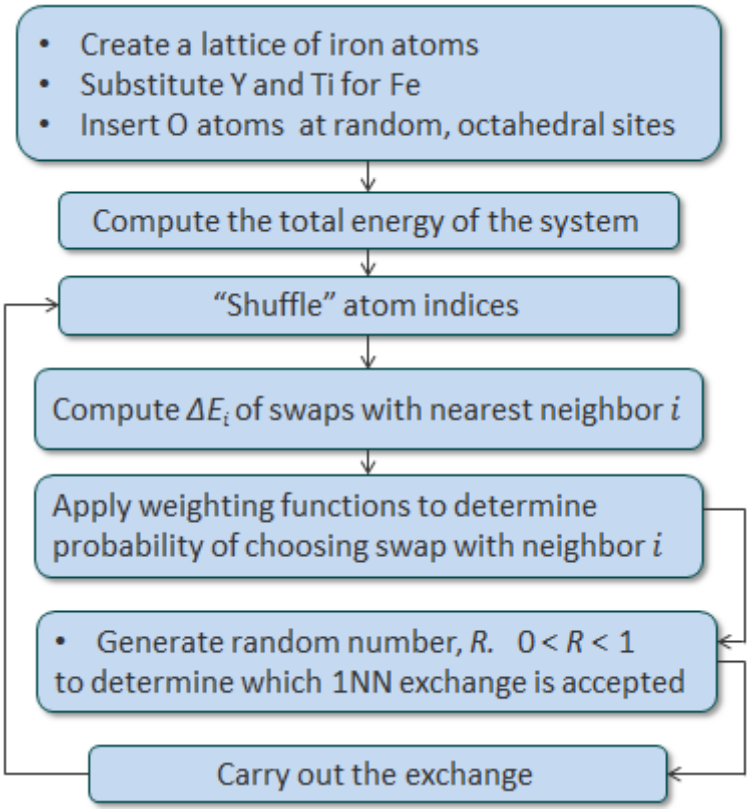


Figure 17. Flow chart explaining On-lattice Monte Carlo method for Ti-Y-O cluster in iron

As shown in Figure 17, the on-lattice simulation is initiated by placing titanium, yttrium, and oxygen in an iron lattice and computing the total energy of the system. The atom indices are scrambled, and for each particular atom, the change in energy resulting from a nearest neighbor swap is calculated for each of its nearest neighbors. Weighting functions are applied to determine which nearest neighbor swap will be chosen. The atom indices are then shuffled once again to repeat the process. In the off-lattice relaxation, atoms are swapped with nearest neighbors, but moves may be rejected based on the resulting change in energy. A disadvantage of using the off-lattice algorithm is that the

minimizations that are performed each iteration take on the order of a second, making the simulation very costly due to computing time. However, this type of simulation can provide a more realistic view of the formation of the cluster since swaps that are not likely to occur are rejected based on the change in energy that would result in accepting the swap. This served as motivation for the off-lattice simulation of a Ti-Y-O cluster in iron.

Off-lattice Monte Carlo simulations were run with a cluster of Ti, Y, and O within an iron lattice. Also present at the beginning of the simulation were dispersed impurities of Ti, Y, and O throughout the simulation box. The temperature was set to 1273 K and the simulation run for 250,000 steps. Figure 18 shows the last frame of the on-lattice simulation of the cluster as well as the last frame of the off-lattice simulation. Yellow atoms represent yttrium, blue atoms are titanium, and red atoms are oxygen.

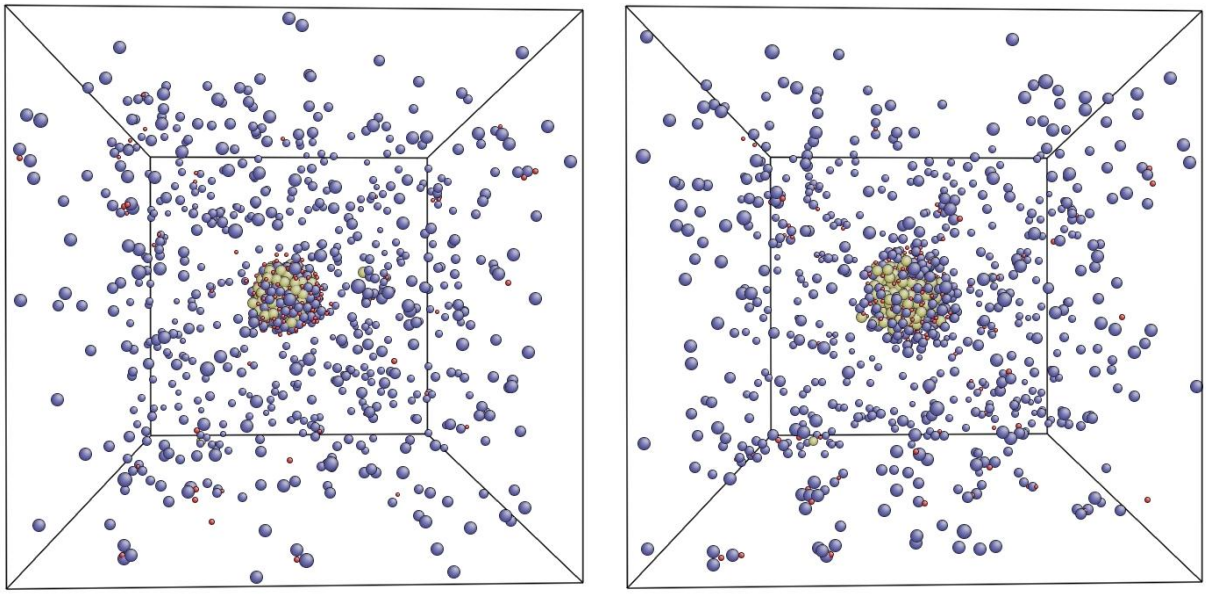

Figure 18. Last frames of On-lattice Monte Carlo (left) and Off-lattice Monte Carlo (right) simulations of Ti-Y-O nanoclusters in iron

The results of the off-lattice relaxation of the on-lattice structure show that the Ti-Y-O cluster is less confined to the on-lattice positions. The cluster does not change significantly in size, but it is represented in a less compact or stressed state. After the off-lattice relaxation, more titanium atoms have joined the periphery of the cluster. The end state of the off-lattice relaxation was used in the following study of the effects of radiation on the nanoclusters in iron matrices.

# CHAPTER 4:
# RADIATION STABILITY OF TI-Y-O CLUSTER IN IRON

The presence of Ti-Y-O nanocluster precipitates may strengthen pure iron in irradiated environments. This is likely due to the high number of impurities introduced in the nanostructure which create a high density of sites for the recombination of defects. These sites also hinder the growth of defects by inhibiting their combination. An important component in the study of nanostructured ferritic alloys is their resistance to radiation damage. In order to study the effects of radiation on these clusters, this thesis will focus on the number of defects produced by incident radiation as well as the average number of atoms displaced by more than 0.5 nm as a result of an incident radiation particle.

In order to study the behavior of Ti-Y-O nanoclusters under radiation, displacement cascade simulations were conducted. In a displacement cascade simulation, a chosen atom is given kinetic energy as if it were the target of an incident radiation particle. The chosen target atom is the first atom encountered by the incoming radiation particle and is called the primary knock-on atom, or PKA. Energy from the incident radiation particle is imparted to the PKA and causes the PKA to move from its original position; the PKA may then displace other atoms within its path.

In the cascade simulations in this work, the chosen PKAs were either within the Ti-Y-O cluster, on the outer layer of the cluster, or in the surrounding layers of BCC iron. For simulations in which the PKAs were on the outer layer of the cluster or in surrounding iron layers, the velocity of the PKA was assigned such that the direction of the atom was toward

the Ti-Y-O cluster at the start of the cascade. Simulations were performed involving four types of PKAs: a yttrium atom near the center of the Ti-Y-O cluster, a titanium atom near the center of the cluster, an iron atom near the outer layer of the cluster, and an iron atom several layers outside the cluster. Each simulation was performed using five different initial velocity directions at energies of 10keV and 20keV. A control simulation was also performed in which a yttrium atom was given an initial velocity consistent with an energy of 20 keV in pure iron.

For each type of simulation run, the results of the number of iron interstitials and vacancies were recorded. Plots were then made containing the average number of defects produced in the cascade. Similar plots were also made containing the average displacement of atoms resulting from the cascade. These plots are shown in the figures which follow.

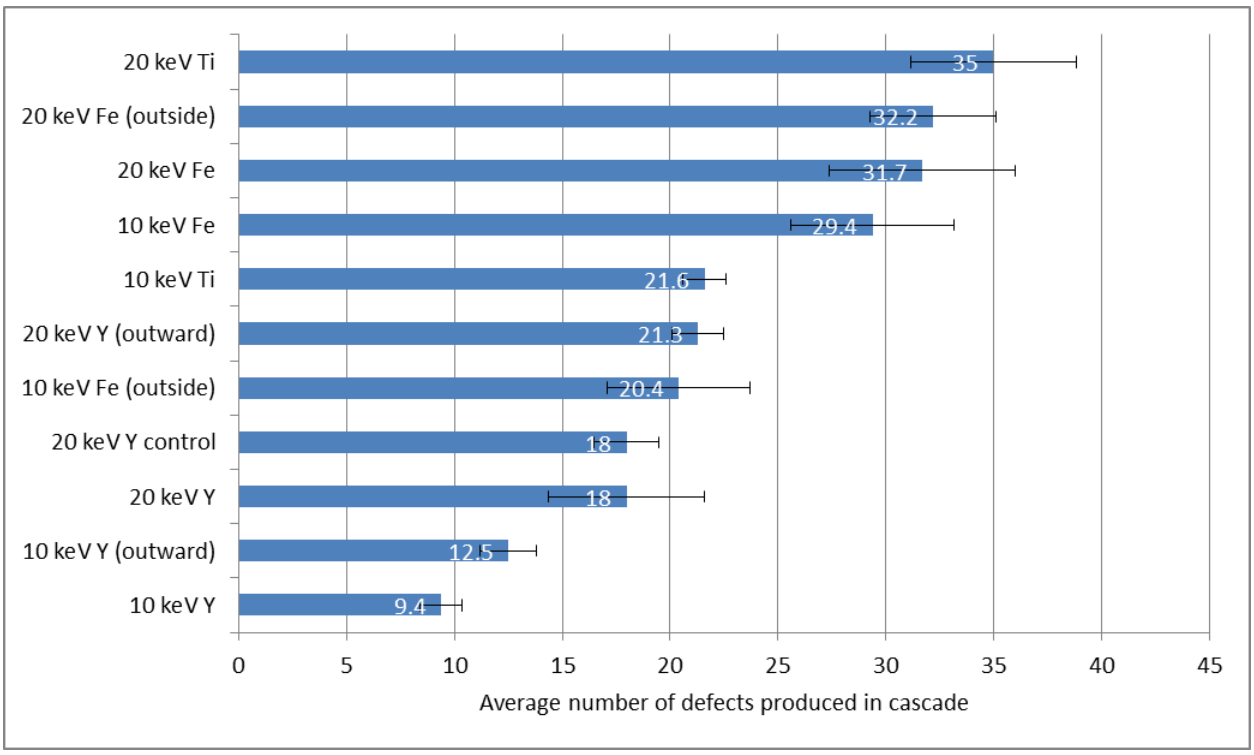


Figure 19. Average number of defects produced in a cascade in a Ti-Y-O cluster in iron

Figure 19 shows the average number of defects produced in each cascade study. The highest number of defects occurred in the 20 keV titanium cascade. Considering the error bars, however, this could be said for the 20 keV iron cascade initiated outside the cluster as well as for the 20 keV iron cascade inititated on the periphery of the cluster. The lowest numbers of defects produced were in the cascades initiated on yttrium atoms inside the cluster. While the number of defects was noticeably lower for Y initiated cascades, it is important to note that it was difficult to quantify the number of defects created within the Y-Ti-O nanocluster due to the substantial distortions of these atoms away from perfect

lattice positions. In addition, the 20 keV cascade initiated on a yttrium atom near the center of the cluster produced about the same amount of defects as were produced in the control simulation containing pure iron.

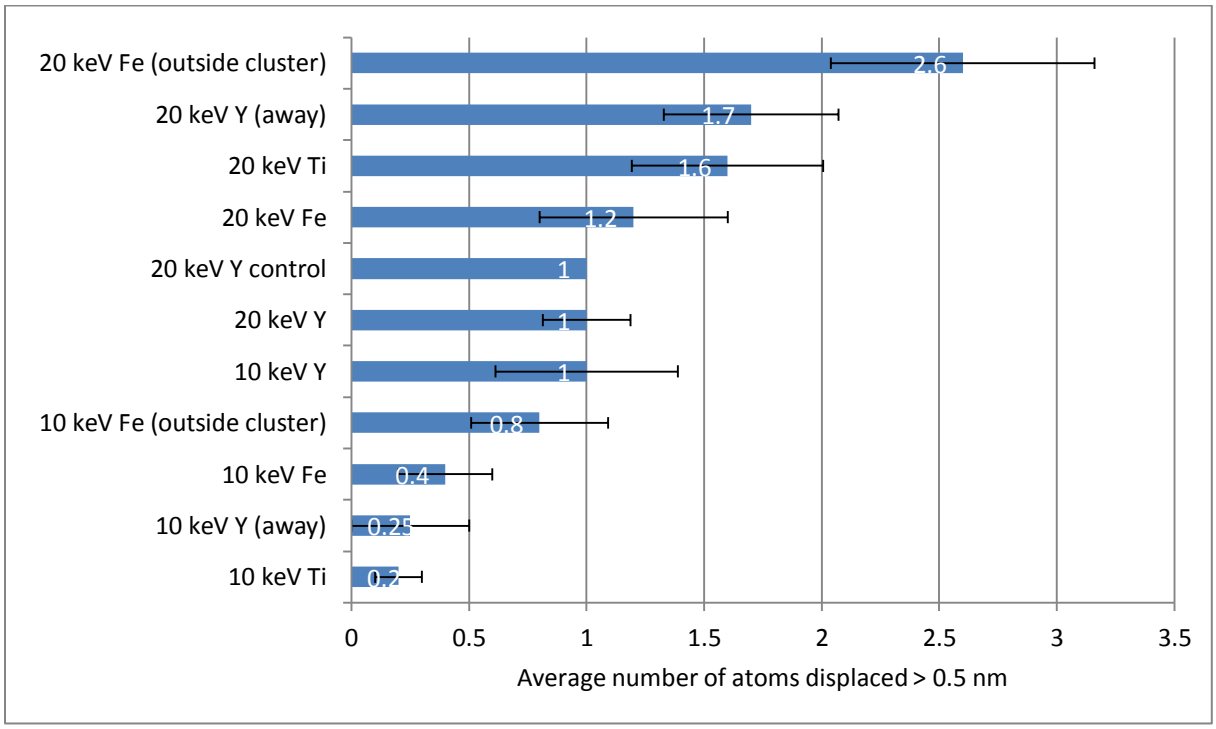


Figure 20. Average number of atoms displaced more than 0.5 nm during the cascade

In Figure 20, the average number of atoms displaced more than 0.5 nm is shown for each cascade simulation. In this figure, the labels “away” and “outside cluster” denote cascades initiated with initial velocity components oriented away from the center of the cluster and cascades initiated outside the cluster, respectively. The 20 keV iron cascade

initiated outside the cluster results in the highest number of atoms displaced. The displacement results of the 20 keV titanium cascade initiated inside the cluster and iron on the periphery of the cluster are also at the top of the chart. When a yttrium atom near the edge of the cluster is the PKA in the 20 keV cascade and its initial velocity is away from the center of the cluster, the average number of atoms displaced more than 0.5 nm is greater than if the yttrium atom were at the center of the cluster. Yttrium at the center of the cluster is seen to again produce a low amount of damage; only one atom, on average, is displacement more than 0.5 nm in a yttrium cascade.

In addition to documenting the number of defects produced in each cascade and the average number of atoms displaced more than 0.5 nm, the number of Ti, Y, or O atoms which left or joined the cluster was also recorded. In some instances, single O atoms were observed leaving the cluster during the cascade. Titanium and yttrium atoms were not disturbed far enough from their positions to leave the periphery of the cluster. From these results, there is no appreciable damage to the cluster as a result of the incident radiation. The composition, size, and structure of the cluster did not change significantly as a result of radiation damage in any of the cascade simulations.

The results of the defect cascade simulations show that the effects of radiation are smallest when a yttrium atom at the center of the cluster is the primary knock-on atom in the radiation event. Also, the highest amount of damage is done when the radiation is incident on an iron atom outside the cluster or near the cluster's edge or a titanium atom in the cluster. It is also noteworthy from the control simulation that there is a comparable number of defects created by a 20 keV cascade in pure iron and a 20 keV cascade initiated

on a Y atom at the center of the Ti-Y-O precipitate cluster. Also, the cascade simulations showed no appreciable changes in the number of atoms of each species contained within the cluster; no appreciable amount of joining or leaving the cluster was observed as a result of the cascades. Given the results of the cascade analyses, there is sufficient evidence to support that the Ti-Y-O precipitate clusters exhibit resistance to radiation damage in iron alloys. For this reason, nanostructured ferritic alloys present themselves as a promising material for use in irradiative environments such as those found in new nuclear reactor concepts and designs.

# CONCLUSION

Nanostructured ferritic alloys possess very desirable mechanical properties under high-temperature, high-radiation environments. These alloys may be of great value in constructing structural components for new nuclear reactor concepts which implement high temperatures and high radiation levels. Researching the formation, structure, and stability of the nanoprecipitates is necessary in order for nanostructured ferritic alloys to be useful in nuclear applications.

The work contained in this thesis served to further investigate the structure and composition of Ti-Y-O nanoclusters in iron as well as the kinetics controlling their formation. This research also investigated the behavior of the nanoclusters in a radiation environment. The results contained in this thesis give insight as to the diffusivity of oxygen interstitials in body-centered cubic iron as well as the activation energy for diffusion for oxygen in an iron lattice. Binding energies of oxygen interstitial and substitutional atoms with iron vacancies were also documented. Small oxygen clusters were studied to determine the temperatures at which they dissociate as well as whether the presence of iron vacancies affects whether oxygen atoms remain bound in small clusters. The cluster formation energies for yttria and titania were also documented in this thesis. Off-lattice relaxations and displacement cascades were performed on an existing Ti-Y-O cluster in iron.

From simulations of oxygen diffusion in body-centered cubic iron, the diffusion coefficient of a single oxygen interstitial atom in iron was found to be $3.4 \times 10^{-5}$ $cm^2s^{-1}$ at

2500 K and an activation energy for diffusion of 0.064 eV. A di-oxygen interstitial atom in iron was found to have a diffusion coefficient of 2.95 x $10^{-5}$ $cm^2s^{-1}$ at 1000 K and an activation energy for diffusion of 0.293 eV. The binding energy calculations showed that small oxygen clusters in iron are most stable in the presence of a yttrium atom; however, titanium proved to provide stability in small oxygen clusters as well. Thus, yttrium and titanium were found to increase the binding energy of small oxide clusters in iron. Simulations of small oxygen clusters showed that clusters of two oxygen interstitials and one iron vacancy are bound at 1000 K but dissociate at a temperature of 1700 K on a time scale of five nanoseconds. A small cluster of two interstitial oxygen atoms and a titanium atom was also bound at 1000 K but dissociated at 1700 K on this time scale. Clusters of two interstitial oxygen atoms and a yttrium atom were found to be bound at both 1000 K and 1700 K. A cluster of three interstitial oxygen atoms was found to dissociate at 1200 K; clusters of three oxygen interstitials plus one or two iron vacancies also dissociated at 1200 K. This showed that, on the 5-ns time scale, tri-oxygen interstitial clusters are not bound at this temperature, regardless of the number of iron vacancies in the cluster.

The diffusion coefficients found using the simple pairwise interatomic energy potentials agreed well with the documented values [9] for oxygen diffusion in iron. Also, the formation energies of Ti-O and Y-O clusters in iron compared well with the formation energies documented in a previous study [2]. The values for diffusion coefficient and formation energies of oxygen and small oxide clusters in iron agree with other documentation; this serves to validate the energy potentials used in this thesis.

In the cascade analyses performed in this work, the least damage was shown to occur from a cascade in which the primary knock-on atom was a yttrium atom near the center of Ti-Y-O cluster. This is significant in that it may show that yttrium aids in stabilizing the cluster under radiation. Cascades initiated on a titanium atom in the Ti-Y-O cluster also resulted in small amounts of defect production, hinting to the fact that titanium may also contribute to radiation resistance. In the cascades performed, no significant amount of Ti, Y, or O atoms left or joined the cluster. The size and composition of the structure were not changed significantly by any of the cascades. This alludes to the fact that these precipitate clusters are resistant to damage caused by incident radiation.

The results and analyses presented in this thesis indicate that nanostructured ferritic alloys are valuable in fabricating structural materials in new concept nuclear reactors such as the gas-cooled fast reactor, molten salt reactor, and fusion reactors. The high temperatures and radiation levels Ti-Y-O clusters can withstand make them great candidates for use in reactor materials. Given the body of work presented in this thesis, there remains future work to accomplish in the study of nanostructured ferritic alloys. In the study of the oxygen-vacancy binding energies, it may be important to also study the binding energies of small yttrium-oxygen and titanium-oxygen clusters. These binding energies may also be important in the growth and retention of small Ti-Y-O clusters. Also, the dissociation of small oxygen clusters should be documented as a probability of dissociation as a function of temperature and time since the two temperatures studied in this thesis are not grounds for making broad assumptions as to whether a cluster dissociates at a given temperature.

# List of References

1. Nanstad, R.K., et al., *High temperature irradiation effects in selected Generation IV structural alloys.* Journal of Nuclear Materials, 2009. **392**(2): p. 331-340.
2. Barnard, L., et al., *An ab initio study of Ti-Y-O nanocluster energetics in nanostructured ferritic alloys.* Acta Materialia, 2012. **60**(3): p. 935-947.
3. M.J. Alinger, G.R. Odette, and D.T. Hoelzer, *The development and stability of Y-Ti-O nanoclusters in mechanically alloyed Fe-Cr based ferritic alloys.* Journal of Nuclear Materials, 2004. **329-333**: p. 382-386.
4. M.J. Alinger, G.R. Odette, and D.T. Hoelzer, *On the role of alloy composition and processing parameters in nanocluster formation and dispersion strengthening in nanostructured ferritic alloys.* Acta Materialia, 2008. **57**: p. 392-406.
5. Miller, M.K. and D.T. Hoelzer, *Effect of neutron irradiation on nanoclusters in MA957 ferritic alloys.* Journal of Nuclear Materials, 2011. **418**: p. 307-310.
6. Hammond, K.D., et al., *Simple pair-wise interactions for hybrid Monte Carlo–molecular dynamics simulations of titania/yttria-doped iron.* Journal of Physics: Condensed Matter, 2013. **25**(5): p. 055402.
7. *LAMMPS*. Available from: http://lammps.sandia.gov.
8. R.B. Bird, W.E.S., E.N. Lightfoot, *Transport Phenomena*1976: John Wiley & Sons.
9. Barlow, R. and P.J. Grundy, Journal of Materials Science, 1969. **4**: p. 797.

# VITA

Natalie Browning Camilli was born in Knoxville, TN to the parents of Denise Dotts-Browning and William Gregory Browning. She attended Karns High School, where she was the president of the school's chapter of the National Honor Society and a member of the track team and band. She attended college at the University of Tennessee at Knoxville, where she earned a Bachelor of Science degree in Nuclear Engineering in May of 2012. She accepted a Graduate Research Assistant position within the Nuclear Engineering Department at the University of Tennessee in 2012. Natalie will earn a Master of Science degree in Nuclear Engineering in May of 2013.